

ELECTROCHEMISTRY IN NEAR-CRITICAL AND SUPERCRITICAL FLUIDS

PART V. THE DIMERIZATION OF QUINOLINE AND ACRIDINE RADICAL ANIONS AND DIANIONS IN AMMONIA FROM -70°C TO 150°C

RICHARD M. CROOKS and ALLEN J. BARD

Department of Chemistry, The University of Texas, Austin, TX 78712 (U.S.A.)

(Received 8th July 1987; in revised form 7th September 1987)

ABSTRACT

An experimental apparatus capable of supporting electrochemical measurements in ammonia at high temperatures and pressures is described. The dimerization reactions of the radical anions of quinoline and acridine were studied over a 220°C temperature range in ammonia. The cyclic voltammetric and chronoamperometric experiments were analyzed by the theory for reversible dimerizations. At low temperature the dimerization was totally irreversible, but at elevated temperatures the rate of the back reaction was significant and the dimerization reaction was facile. The rates of the dimerization reactions were extrapolated to very high temperature and were found to be in qualitative agreement with cyclic voltammetric results in supercritical ammonia. The activation energies for the dimerization reactions are reported. The diffusion coefficients of quinoline and acridine from -70°C to 150°C are reported.

INTRODUCTION

In the first four papers of this series, we discussed the electrochemistry of a number of inorganic and organic substrates in near-critical and supercritical ammonia [1] and water [2]. The focus of the earlier papers was primarily on experimental techniques, simple electron transfer reactions, and qualitative descriptions of electrochemically initiated homogeneous reactions. For example, we described the electrochemistry of nitroaromatic compounds, solvated electrons, and a homologous series of diaza-aromatics (pyrazine, quinoxaline and phenazine) in ammonia from 25 to 150°C at vapor pressures of 0 to 300 bar [1b]. For the diaza-aromatics, the electron transfer reactions remained reversible, or nearly reversible, throughout this temperature range; and the anion radicals, and the dianion in the case of phenazine, were stable on the cyclic voltammetric (CV) time scale.

The purpose of the current investigation is to extend these preliminary studies by exploring the effects of a broad range of pressure and temperature on the thermody-

namics and kinetics of the electrochemically initiated dimerization of the radical anions of quinoline (Q) and acridine (A). For example, the dimerization of $Q^{\cdot-}$, the radical anion, in ammonia, which is irreversible at -40°C , might be shifted into different kinetic regimes at higher or lower temperature, or might be supplanted entirely by a new process, such as polymerization or protonation. For the current study, we were able to access temperatures from -70 to 150°C and pressures from 0 to 300 bar. To our knowledge, this is the broadest temperature range over which an electrochemically initiated homogeneous reaction has been studied by electrochemical techniques. In a previous paper [1b], we discussed the properties of supercritical fluids (SCF) and how they can be used to advantage as electrochemical solvents. In addition, a number of recent reviews have appeared that cover the solution properties of SCF with particular emphasis on separations and solubility [3]. From an electrochemical viewpoint the most important property of the SCF is its combination of gas-like compressibility and liquid-like density. Compression of the SCF permits tuning of the solvating power through a broad range, because of changes in density (ρ) and dielectric constant (ϵ). A dimerization reaction was chosen for this study because it should be sensitive to changes in these parameters.

Quinoline

The electrochemical reduction of Q has been studied previously in acetonitrile (AN) [4] dimethylformamide (DMF) [5], and ammonia [6a,b]. In dry, aprotic media, two one-electron waves appear corresponding to the formation of $Q^{\cdot-}$ and the dianion, Q^{2-} . In ammonia at -40°C [6a,b] and AN at 25°C [4], $Q^{\cdot-}$ and Q^{2-} undergo a dimerization reaction. The suggested mechanism in ammonia is given in Scheme 1. Here the electron transfers were assumed to be reversible and the chemical dimerization was found to be irreversible. The forward rate constant (k_2) for the irreversible dimerization of $Q^{\cdot-}$ in ammonia at -40°C was estimated as 1.5×10^2 [6a] and $4.0 \times 10^2 \text{ M}^{-1} \text{ s}^{-1}$ [6b].

The importance of K^+ to the dimerization reaction of pyridine in ammonia has been demonstrated [7a]; when the tetra-n-ethylammonium ion replaced K^+ as the electrolyte cation, k_2 fell by two orders of magnitude. Thus the dimerization illustrated in Scheme 1 relies on ion pairing. The reduction of Q by chemically generated solvated electrons (e_s^-) in tetrahydrofuran (THF, $\epsilon = 8$) resulted in the formation of 99% dimeric dianion as verified by ESR [6c]; but in

SCHEME 1



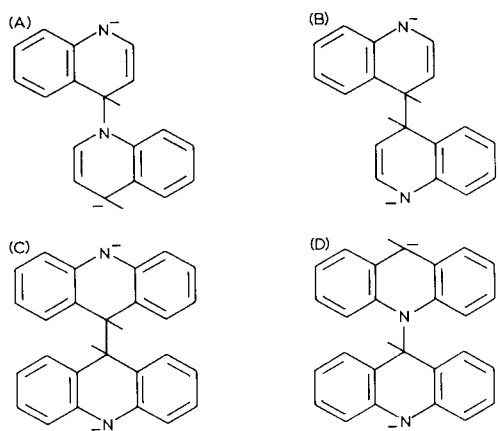


Fig. 1. Suggested structures for the coupled radical anions of quinoline and acridine. (A) 4-Hydro-1',4'-bi-quinolinyl dianion; (B) 4,4'-dihydro-4,4'-biquinolinyl dianion; (C) 9,9'-dihydro-9,9'-biacridinyl dianion; (D) 9-hydro-9,10'-biacridinyl dianion.

hexamethylphosphoramide (HMPA, $\epsilon = 46$), the monomer was formed quantitatively. The shift in equilibrium was correlated to the differences in the dielectric constants and solvating power of the solvents. In DMF the 1,4'-dihydrodimer has been suggested as the structure of the dimer, but conclusive proof is lacking [5]. Pyridine [7b] and pyrimidine [7c] have been shown to dimerize as the 4,4'-complexes in 1,2-dimethoxyethane and AN, respectively. By analogy, it is likely that $Q^{\cdot-}$ forms either the 1,4' or the 4,4' dimer upon reduction in ammonia, Fig. 1.

Acridine

The polarographic reduction of acridine (A) in water has been described [8]. Depending on pH, either two single-electron waves or a single two-electron wave was found; a 9,9'-dihydrodimer was isolated. In DMF two one-electron waves were observed [9a], and similar behavior was found in AN, where the presence of a dimeric species was reported [4]. Compounds related to A have been studied; 9-cyanoanthracene [9b] and 9-carboxyanthracene [9c] were shown to form 9,10' dimers in dimethylsulfoxide (DMSO). Suggested structures for the $A^{\cdot-}$ dimer are shown in Fig. 1. No kinetic data are available for the reduction or following reactions of A in aprotic media, and the electrochemistry of A in ammonia has not been reported previously.

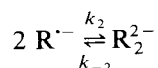
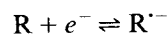
Theory of electrochemically initiated dimerization

Cyclic voltammetry, chronocoulometry, and double potential step chronoamperometry (DPSC) were used to investigate the heterogeneous and homogeneous kinetics and the thermodynamics of Q and A in ammonia between -70 and 150°C

[10]. The general methods for treating homogeneous dimerization reactions following a reversible heterogeneous electron transfer (E_rC_2 mechanism) were described over twenty years ago [10–13]. In previous experiments involving the dimerization of $Q^{\cdot-}$ and $A^{\cdot-}$, the position of equilibrium in the reaction was assumed to be shifted strongly towards the dimer, and the back reaction (monomerization) was not considered. If the rate of the back reaction is significant, however, the reaction must be treated as a reversible process.

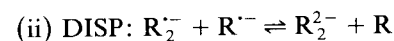
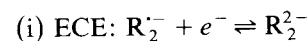
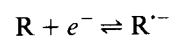
Three possible mechanisms can be considered for the dimerization reaction. These generally follow previous dimerization schemes investigated extensively for the radical anions of activated olefins and related species [14,15]. Using Savéant and Andrieux's notation [15], we can represent these as follows:

(1) The radical–radical coupling mechanism (DIM1):

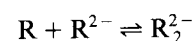
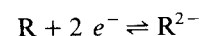


$$K_2 = k_2/k_{-2}$$

(2) The radical–substrate coupling mechanism (DIM2)



(3) The dianion–substrate coupling mechanism (DIM3)



where K_2 is the equilibrium constant for the second order dimerization, and k_{-2} is the rate constant for the back reaction (monomerization). The DIM1 and DIM3 processes are straightforward; however, three distinct cases can be distinguished for DIM2 [14f,g,h,l;16b,c]. The first is the ECE case in which the radical–substrate anion radical dimer, $R_2^{\cdot-}$, is reduced at the electrode surface. The two disproportionation mechanisms arise from the possibility of homogeneous reduction of $R_2^{\cdot-}$ by $R^{\cdot-}$. If the rate determining step (rds) of the DIM2–DISP reaction is coupling of radical and substrate, the process is termed DIM2–DISP1. If the rds is homogeneous electron transfer, a DIM2–DISP2 reaction is defined.

The simple mechanisms described here can be complicated, or their rates altered, by the presence of a proton source, especially water [14j,17]. Since the ammonia, electrolytes, and cells used in this study were easily dried, such complications were avoided. Proton abstraction from the solvent is unlikely, since ammonia remains a weak acid even when supercritical, as demonstrated previously by the stability of the highly nucleophilic phenazine dianion [1b].

In subsequent sections it will be shown that the DIM1 process dominates the homogeneous chemistry of the $Q^{\cdot-}$ and $A^{\cdot-}$ radical anions throughout the temperature range studied. Although the DIM3 mechanism does not apply to the dimerization of the radical anions, a case can be made for a contribution from DIM2. Radical-substrate coupling could occur in some systems [14,18], and a recent demonstration showed unambiguously that concentration induced interconversion between DIM2-DISP1 and DIM2-DISP2 mechanisms was possible [18e]. However, for species related to those of the current work, a pure DIM1 scheme has been shown to apply [14,19,20]. In addition, the results reported here for the dimerization of radical anions follow strictly the theoretical behavior for a pure DIM1 scheme throughout the temperature range studied.

The variations of cathodic peak potential, $E_{p,c}$, with scan rate, v , and bulk concentration, c^* , are especially valuable for reaction mechanism determination. Because of experimental difficulties, we were not always able to acquire sufficiently precise $E_{p,c}$ data to take advantage of these important diagnostics. The potential control problems arise from two sources: first, uncompensated solution resistance; and second, the necessity of using an inherently imprecise quasi-reference electrode. For those reasons, we relied heavily on the more reliable current-based measurements, especially above room temperature, to assign the reaction mechanisms as DIM1.

The voltammetric treatment of the DIM1 case is best summarized by a zone diagram, Fig. 2, developed by Savéant and co-workers [15,20]. The construction of the diagram simplifies the analyses of complex reaction schemes, because only the minimum number of parameters which govern the experimental observables are included for consideration. For the consecutive, reversible dimerization reaction, only two parameters are required to describe the state of the system completely. In some regions of the diagram, limiting behavior obtains in which one or both of the parameters take on very large or very small values. Within these zones the theoretical treatment of the system can be simplified, since fewer parameters need be considered.

The voltammetry of the reversible dimerization reaction is described by a thermodynamic, or equilibrium, parameter: $\chi = 1/K_2c_R^*$; and a kinetic parameter: $\lambda = (RT/F)(k_2c_R^*/v)$, where v is the scan rate, R is the gas constant, T the absolute temperature, F Faraday's constant, and c_R^* the bulk concentration of substrate [15,20]. The zones in Fig. 2 correspond to predicted electrochemical behavior for different values of χ and λ . KG is the most general zone, in that both χ and λ are required to describe the voltammetric response. Analysis of the voltammetry in the KG region is difficult, since analytical expressions that govern the observables (peak current, i_p ; peak potential, E_p ; or wave shape) cannot be derived. At very large values of K_2 , i.e., as $\chi \rightarrow 0$, the reaction depends only on λ ; and at small values of k_2/v , zone KO is obtained. The voltammetry in this zone appears quasi-reversible; when $k_2/v \rightarrow 0$ ($\lambda \rightarrow 0$), reversible behavior (zone DO) is obtained. When k_2/v becomes larger ($\lambda \rightarrow \infty$), totally irreversible kinetics (zone KP) are observed.

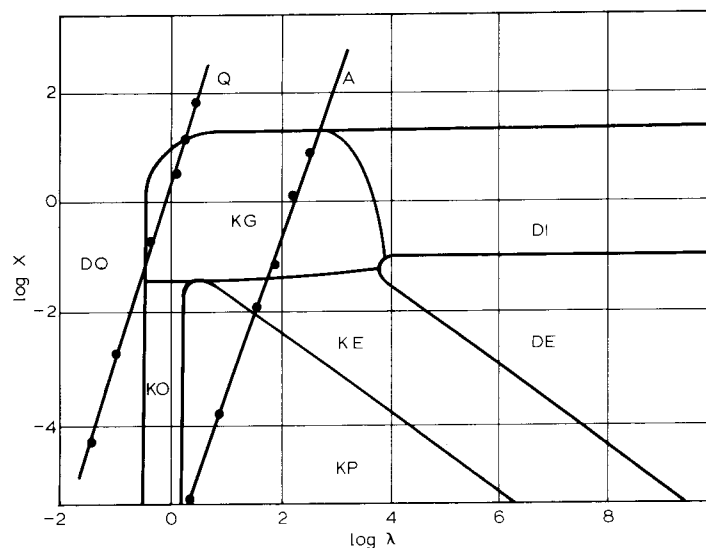


Fig. 2. Kinetic zone for radical-radical dimerization (DIM1). $\chi = 1/K_2 c_R^*$, $\lambda = (RT/F)(k_2 c_R^*/v)$. The lines Q and A represent the kinetic and thermodynamic state of the quinoline and acridine systems over the temperature range studied. The points correspond to the conditions of the voltammetry shown in Figs. 4 and 7 for $v = 1$ V/s. The points nearest the bottom of the figure represent Figs. 4A and 7A, and the topmost points correspond to Figs. 4F and 7F. The plots were constructed by extrapolating the kinetic information in Table 4 to the appropriate temperature. For definitions of the zones see text. (Zone diagram derived from ref. 15, p. 352.)

As λ increases, χ can remain small for significant values of k_{-2} . In this case, the forward and reverse kinetics are sufficiently facile to allow a near equilibrium concentration of monomer at the electrode surface upon scan reversal. This behavior corresponds to zone KE, where the single parameter on which the voltammetry depends is $\lambda^{1/2} \chi^{3/4}$. As was the case for zone KO, the current response in KE appears quasi-reversible. DE appears as a limiting case of KE as $\lambda^{1/2} \chi^{3/4} \rightarrow \infty$. Once again, the voltammetry appears reversible, since the kinetics are completely facile in either direction, and an equilibrium concentration of monomer is maintained in the reaction layer adjacent to the electrode surface. Zone KP appears as the other limiting case of KE ($\lambda^{1/2} \chi^{3/4} \rightarrow 0$). The final zone, DI, pertains uniquely to the dimerization reaction scheme and represents kinetic behavior intermediate between the two diffusion controlled zones, DE and DO, where the current response is controlled solely by the equilibrium parameter, χ . Since this zone does not depend on λ , the voltammetry appears reversible.

From the definitions of λ and χ , the kinetic description of a DIM1 reaction can be moved into different zones, if a wide range of experimental parameters is available (see Fig. 2). For example, variation of v produces movement along the horizontal axis, while either c_R^* or K_2 can be employed to move along the vertical axis. For solutions of relatively high viscosity, such as aqueous solutions at 25°C, v

can easily be varied through five orders of magnitude. Thus, for the most kinetically sensitive region of the zone diagram ($\log \chi = -2$), a system can be characterized quite thoroughly, since it can be forced into either DO, KO, KP, KE or DE by variation of scan rate. Since both χ and λ depend on c_R^* , the latter is not particularly valuable for independent adjustment of χ along the vertical axis. Since K_2 is a strong function of temperature, it can be used effectively to control the equilibrium parameter χ , however, as shown by results presented here. It should therefore be possible to adjust the temperature of a system such that a single experimental model would allow the determination of the reaction mechanism and permit calculation of K_2 , k_2 and k_{-2} . However, the necessarily wide range of v may not be available because of the way solution properties change with temperature. As the temperature of a solution is raised, its viscosity decreases, and the possibility of convection increases, resulting in an increase in the minimum useful value of v . Moreover, solution resistance may increase with temperature, since the dielectric constant falls. Therefore, the fastest scan rates, or step times in the case of DPSC, are limited by the time constant of the cell. In principle, this limitation can be minimized by reducing the area of the electrode. The broadest control is achieved through the use of multiple electrodes encompassing a distribution of areas over 4 or 5 orders of magnitude.

To derive as much kinetic information as possible from the Q and A systems over a broad temperature range, three kinetic regimes were identified, and an appropriate theoretical model was applied to each. A planar electrode, a Nernstian electron transfer, identical diffusion coefficients of the reduced and oxidized substrate [20] and semi-infinite linear diffusion were assumed in all cases.

(1) In zones KO and KP, the dimerization can be considered irreversible. In these zones, encountered in this study at low temperature, the effect of k_{-2} can be neglected; and the theories of Nicholson and co-workers [16a] and Savéant and co-workers [16b] are employed. For cyclic voltammetry the diagnostic criteria for distinguishing between DIM1, DIM2-ECE, DIM2-DISP1, and DIM2-DISP2 in the irreversible case are given in Table 1 [11,15,16b,c]. The useful features are variations in $E_{p,c}$ with c^* and v , and the sensitivity of the current function, i_{fun} , to λ . It is clear from Table 1 that millivolt resolution of $E_{p,c}$ is required to obtain unambigu-

TABLE 1

Summary of diagnostic parameters available from cyclic voltammetry for the analysis of irreversible dimerization reactions [11,15,16b,c]

Reaction type	$\left(\frac{\partial E_{p,c}/\partial \log c^*}{T/302}\right)/\text{mV}$	$\left(\frac{\partial E_{p,c}/\partial \log v}{T/302}\right)/\text{mV}$	$\Delta i_{fun}^a/\%$
DIM1	20	-20	+18
DIM2-ECE	30	-30	-4
DIM2-DISP1	30	-30	+3
DIM2-DISP2	20	-20	+6

^a Δi_{fun} is the percentage change in the current function, $i_{fun} = i_{p,c}/(v^{1/2} - c_R^*)$, as λ is increased over the complete kinetic range.

ous kinetic information from potential measurements. As discussed (vide supra), such precision is not generally obtained in the high temperature/high pressure system described here. Therefore, the utility of the potential dependent functions listed in Table 1 was of secondary importance compared to current-based measurements for mechanistic evaluation. For example, the ratio of the anodic to cathodic peak current ($i_{p,a}/i_{p,c}$) is closely related to k_2 , since some of the R'^- will dimerize and will not be oxidized upon scan reversal. If τ is the time between the standard potential and the switching potential $(E_\lambda - E^\circ)/v$, then for DIM1:

$$k_2 = \omega / \{ c_R^* \tau 10^{0.034(a\tau-4)} \} \quad (5)$$

where ω is a dimensionless parameter related to $i_{p,a}/i_{p,c}$ through a theoretical working curve, a is a dimensionless scan rate parameter ($a = nFv/RT$), and n is the number of electrons transferred [16a].

(2) In zones KE and KG, found at moderate to high temperatures, the effect of the back reaction must be accounted for through the equilibrium constant K_2 . In this zone Savéant's treatment based on DPSC was applied [20]. DPSC involves potential excursions from a region where $i = 0$ to the plateau of the cathodic wave for a time θ , followed by a step back to the plateau of the anodic wave. Under these conditions, only mass transfer and homogeneous kinetics need be considered, which removes the necessity of considering heterogeneous kinetics or small potential control errors. For an electron transfer that results in a stable product, the ratio of the currents measured at the end of the negative-going step ($t = \theta$) and again at $t = 2\theta$, is $R_r = i(2\theta)/i(\theta) = 0.293$. A dimensionless, normalized value of this ratio, R , will be used throughout this discussion where $R = [i(2\theta)/i(\theta)]/R_r$. $R = 1$ in zones DO and DE, and $R = 0$ in zone KP. R has intermediate values in zones KO and KE.

The complete theoretical treatment of the DPSC technique, as applied to Scheme 1, can be described by a zone diagram similar to that shown in Fig. 2 (ref. 20, Fig. 3). The experimental evaluation of K_2 , k_2 and k_{-2} is made by constructing a plot of R vs. θ . Either the maximum or minimum of this plot is compared to a working curve (ref. 20, Fig. 8), from which the magnitude of κ is obtained. The magnitude of k_2 can be calculated from λ , which can be estimated from a set of working curves (ref. 20, Fig. 1) and the rate constant of the back reaction calculated from $K_2 = k_2/k_{-2}$.

(3) In zones DE and DO, the following reversible reaction is not manifested in either $i_{p,a}/i_{p,c}$ or R , because of either very fast kinetics of the back reaction (high temperature, zone DE) or very slow kinetics of the forward reaction (low temperature, zone DO). The cyclic voltammetry in zone DO is that expected for an uncomplicated Nernstian reaction [1b,21]. Zones DO and DE can only be distinguished through the variation of peak potential with concentration. In DO, $E_{p,c}$ is independent of c_R^* , while in DE [15]:

$$\partial E_{p,c} / \partial \log c_R^* = 30(T/302) \text{ mV} \quad (6)$$

In both zones $E_{p,c}$ is independent of v [14f,16b]. Under our experimental conditions, we were unable to access zone DE, and thus it is not discussed further.

EXPERIMENTAL

Cells and electrodes

The high pressure/high temperature cell (type 2 cell) used for most of these experiments, shown in Fig. 3, is different from the one used previously (type 1 cell) [1b], because the earlier cell was difficult to clean and dry thoroughly. For the experiments described here, difficulties were encountered with even very low concentrations of oxygen, water, or other impurities, especially at high temperature. While the cell used here was easy to clean and dry, it was not provided with an independent means of pressurization, as was the earlier cell. This represents a limitation to the types of experiments which can be done, since the variation of solution density above the critical point is precluded. Instead, the pressure in the

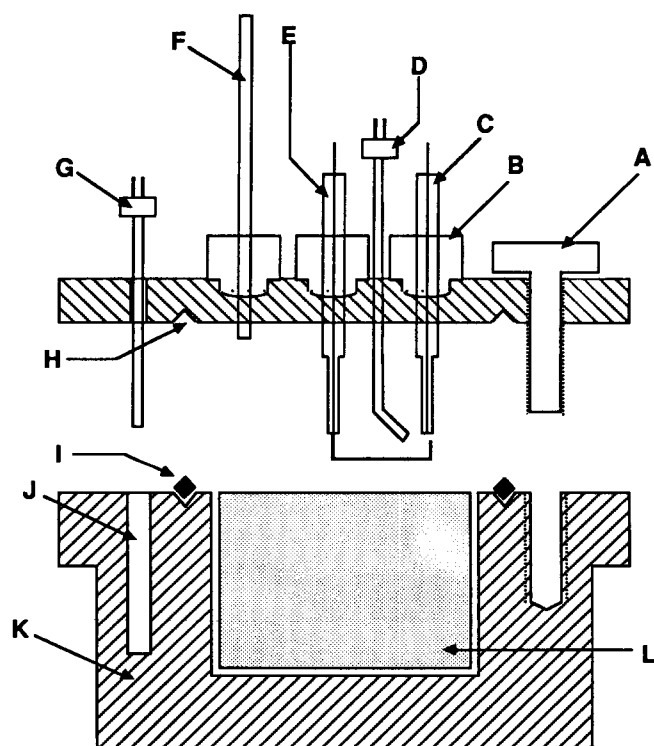


Fig. 3. Cross sectional view of the high pressure/high temperature electrochemical cell (Type 2). (A) Closure bolt (grade 6; 5/16-24); (B) 1/4 inch Taper SealTM to 1/4 inch NPT adapter; (C) tungsten disk working electrode; (D) internal thermocouple; (E) silver quasi-reference electrode; (F) stainless steel tubing for connection to vacuum line and pressure sensor; (G) external thermocouple (to temperature controller); (H) gasket groove; (I) metal gasket; (J) thermocouple well; (K) stainless steel cell body; (L) PyrexTM liner.

cell follows the vapor pressure (coexistence) curve of ammonia up to the critical temperature (T_c). Above T_c the pressure is determined by the volume of the cell and the mass of ammonia originally present.

The design of the type 2 cell is based on a commercially available high pressure bomb (model No. 4651, Parr Instruments, Moline, IL). The base of the cell was made of 316 stainless steel, and the cylindrical interior had a volume of ca. 75 ml. A glass liner fitted to the interior prevented contamination of the solution by corrosion products of the metallic cell at subcritical temperatures. Above the T_c , the solution contacted all interior portions of the cell. A detachable lid, also of stainless steel, was tapped with tapered pipe threads (NPT) to provide for a number of feedthroughs. The halves of the cell were attached to each other by means of a flange arrangement and a stainless steel diamond-shaped gasket (Parr Instruments). Taper Seal to NPT adapters (High Pressure Equipment, Erie, PA) were screwed into the lid to accommodate the electrodes and other hardware necessary for these experiments [1b].

Unlike the type 1 cell, this cell was not able to accommodate more than a single working electrode. For reasons described earlier, it is advantageous to use several working electrodes with different areas. Despite these two limitations, this cell was adequate for obtaining reliable data from ammonia solutions between -70 and 150°C . Both cells showed similar behavior at room temperature where impurities have little effect. With the type 1 cell at 25°C , changes in kinetic and thermodynamic parameters were not changed significantly by pressure changes over the range 1 to 300 bar.

The previously described 1 mm diameter tungsten disk working electrode ($A = 0.0083\text{ cm}^2$) was used for most measurements [1b], but occasionally a tungsten ultramicroelectrode (UME) was used for fast scan rates. A slight modification of the electrode construction procedure permitted fabrication of tungsten and platinum ultramicroelectrodes (UME). The following modification was applied for tungsten UME with areas in the 10^{-4} cm^2 range. Before sealing the tungsten rod into uranium glass, the tip was ground mechanically to a sharp point, then etched further by heating the rod and plunging the tip into crystals of KNO_2 . This resulted in a highly exothermic reaction that vaporized the tungsten rod slowly and caused the tip to become quite sharp. The modified rod was then subjected to the procedure described previously for construction of the finished electrode [1b]. The glass near the tip of the electrode was carefully ground until metal was encountered, then polished as described. Since the area of the electrode was small, it was important that no air bubbles were present at the metal/glass interface. This was easily checked under a microscope, and polishing was continued until a bubble-free region was encountered.

A second type of modification of the basic procedure allowed fabrication of even smaller area (ca. 10^{-5} cm^2) disk electrodes of either tungsten or platinum. Platinum or tungsten wires (Alfa-Products, Danvers, MA) $25\text{--}100\ \mu\text{m}$ in diameter were sealed in Pyrex 7052 capillaries by the same technique as used for the tungsten rods. The glass sheathed wires could then be sealed to the Pyrex portion of the Kovar to Pyrex seal (Ace Glass, Vineland, NJ). Construction was completed as described previously

[1b]. Although the coefficient of expansion of Pyrex 7052 is not well matched to either tungsten or platinum, the small diameter of the wire permitted an excellent seal. (When wires with diameters larger than 100 μm were used, the glass/metal seal separated upon cooling and the electrochemical response was unacceptable.)

Procedure

The cell was carefully cleaned and dried. The working electrode was polished and attached to the lid prior to assembly to allow proper positioning of the reference electrode. The sheath of the ungrounded thermocouple served as the counter electrode. After attaching the lid, pressure transducer, and associated hardware, the cell was placed in a heating mantle and attached to the vacuum line. The cell was evacuated for at least 24 h at 100 °C or until a vacuum of 10^{-6} Torr was obtained; then it was moved into an inert atmosphere box for addition of electrolyte and substrate. After reconnecting the cell to the vacuum line, sufficient ammonia was distilled directly into the cell to obtain a pressure of ca. 300 bar at 150 °C. The prepared cell was disconnected from the vacuum line and placed in a heating mantle (for experiments above room temperature) or a dry ice bath (for low temperature experiments). All experiments were done with a constant mass of ammonia.

Chemicals

The preparation of ammonia and the electrolyte, $\text{CF}_3\text{SO}_3\text{K}$, has been described [1b]. Occasionally, the tetra-*n*-butyl ammonium (TBA) salt of $\text{CF}_3\text{SO}_3\text{H}$ was used as supporting electrolyte. $\text{CF}_3\text{SO}_3\text{TBA}$ (Alfa Products, Danvers, MA) was dried in vacuum at room temperature for 2 days and used without further purification. $\text{CF}_3\text{SO}_3\text{TBA}$ was not stable in ammonia above 100 °C. Quinoline (Aldrich, Milwaukee, WI) was vacuum distilled twice and stored over neutral alumina (Woelm Pharmacia). The purity was verified as better than 99.5% by GC-MS analysis. Acridine (Aldrich) was vacuum sublimed twice. Both were stored in an inert atmosphere box until needed.

Electrochemical measurements

The cyclic voltammetric and chronocoulometric techniques used were described previously [1b]. The DPSC measurements were made as follows. The potential was held at least 200 mV positive of $E_{\text{p,c}}$, and any residual current was allowed to attain a steady state value. The potential was stepped at least 200 mV past $E_{\text{p,c}}$ for a time θ , and then 200 mV positive of $E_{\text{p,a}}$. The potential was occasionally stepped further negative or positive to ensure that heterogeneous kinetics or other processes did not contribute to the current response. The residual current was subtracted from $i(\theta)$ and $i(2\theta)$. In some cases, iR feedback was used. θ ranged from 5 to 1000 ms, but only smaller values were used at higher temperatures, because of convective interference in the desired diffusional response.

The reported values of $E_{1/2}$ were either corrected for kinetics or obtained in DO where $E_{p,c}$ was independent of v and c_R^* . Where this was not possible, as in zone KG, the uncorrected value of $E_{p,c}$ is reported. All potentials are precise to ± 10 mV and are reported vs. the onset of e_s^- generation, as described previously [1b]. Concentrations were corrected for the change in density of the solvent with temperature. Temperatures were controlled to $\pm 2^\circ\text{C}$ and pressure was controlled to ± 2 bar. In zone DO, $i_{p,a}/i_{p,c}$ was calculated by a semiempirical technique for Nernstian electron transfers resulting in stable product [22]. In zones KP and KO, the current ratio was determined by the theoretical method described by Nicholson and co-workers for irreversible dimerization following electron transfer [16a]. In other zones the current ratio was obtained experimentally by measuring $i_{p,a}$ from the $t^{-1/2}$ decay of the cathodic electron transfer [21b]. The precision of the current ratio measurements was estimated to be $\pm 5\%$.

RESULTS AND DISCUSSION

Cyclic voltammetry

Cyclic voltammograms for the first reduction of quinoline in the presence of K^+ from -70°C to 150°C are shown in Fig. 4, and the voltammetric data are summarized in Tables 2 and 3. At the lowest temperatures, Figs. 4a,b, the voltammetry is similar to that described previously for the reduction of Q in ammonia [6a,b]. The large cathodic wave at ca. $+0.80$ V is due to the single electron reduction of Q (eqn. 1), and the corresponding anodic wave is due to the oxidation of $\text{Q}^{\cdot-}$. A second anodic wave, present about 1.1 V positive of this couple, is due to oxidation of the ion-paired dimer:



$\partial E_{p,c}/\partial \log v$ is -19 and -16 mV/decade at -40 and -70°C , respectively, compared to the theoretical values of -15 and -13 mV/decade for a totally irreversible DIM1 process (zones KP, KO). These slightly high values are probably due to either a small uncompensated resistance or the fact that the dimerization is not totally irreversible at all v . The change of the current function at -40 and -70°C (16–22%) is consistent only with the change expected for a DIM1 reaction in zones KO and KP, Table 2.

The change in magnitude of $i_{p,a}/i_{p,c}$ with v at -40 and -70°C is listed in Table 2; Nicholson et al.'s method [16a] described previously was used to correlate this variation to the rate constant for the irreversible dimerization of $\text{Q}^{\cdot-}$. Average values of $k_2 = 1.1 \times 10^3$ and $4.3 \times 10^2 \text{ M}^{-1} \text{ s}^{-1}$ were found at -40 and -70°C , respectively. The value at -40°C is higher than those previously reported, 1.5×10^2 and $4.0 \times 10^2 \text{ M}^{-1} \text{ s}^{-1}$ [6a,b]. The discrepancy in the first case appears to be a calculation error [6a], because the switching potential, E_λ , would have been well into the second reduction of Q to obtain the reported k_2 . If a more reasonable value of E_λ is considered, the reported data indicate a dimerization rate more in line with the one reported here.

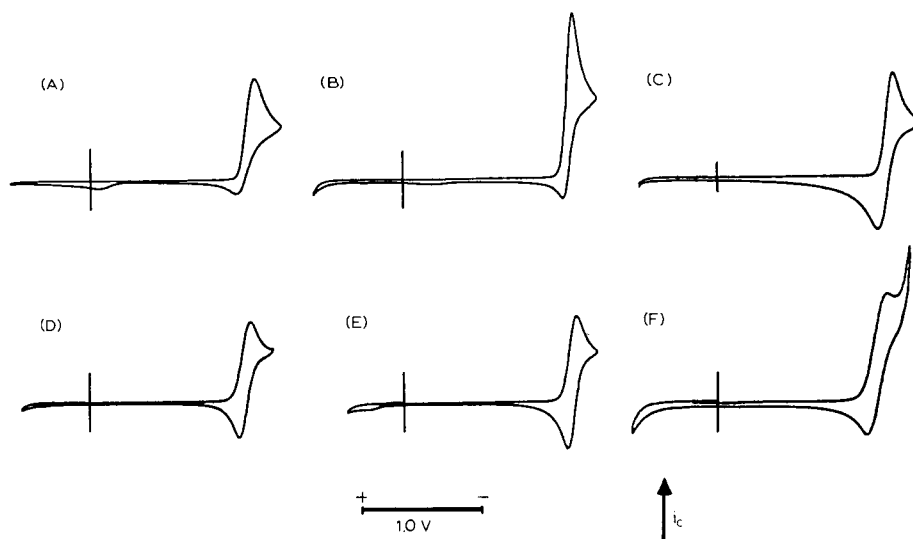


Fig. 4. Cyclic voltammetry of the first reduction of quinoline (Q) in ammonia + $\text{CF}_3\text{SO}_3\text{K}$ at a tungsten working electrode ($A = 0.0083 \text{ cm}^2$) between -70°C and 150°C . (A) $T = -70^\circ\text{C}$, $P = 0.10 \text{ bar}$, $[\text{Q}] = 5.67 \text{ mM}$, $E_{1/2} = +0.800 \text{ V}$, $v = 0.20 \text{ V s}^{-1}$; (B) $T = -40^\circ\text{C}$, $P = 0.70 \text{ bar}$, $[\text{Q}] = 5.39 \text{ mM}$, $E_{1/2} = +0.815 \text{ V}$, $v = 0.20 \text{ V s}^{-1}$; (C) $T = 20^\circ\text{C}$, $P = 8.1 \text{ bar}$, $[\text{Q}] = 4.77 \text{ mM}$, $E_{1/2} = +0.617 \text{ V}$, $v = 0.20 \text{ V s}^{-1}$; (D) $T = 70^\circ\text{C}$, $P = 34 \text{ bar}$, $[\text{Q}] = 4.01 \text{ mM}$, $E_{1/2} = +0.549 \text{ V}$, $v = 0.50 \text{ V s}^{-1}$; (E) $T = 100^\circ\text{C}$, $P = 61 \text{ bar}$, $[\text{Q}] = 3.65 \text{ mM}$, $E_{1/2} = +0.474 \text{ V}$, $v = 0.50 \text{ V s}^{-1}$; (F) $T = 150^\circ\text{C}$, $P = 300 \text{ bar}$, $[\text{Q}] = 3.34 \text{ mM}$, $E_{1/2} = +0.400 \text{ V}$ (estimated), $v = 1.0 \text{ V s}^{-1}$. The concentration of $\text{CF}_3\text{SO}_3\text{K}$ was 0.20 M at -70°C , and fell to 0.12 M at 150°C because of the decrease in solvent density. The current scale is indicated by the height of the vertical mark on each figure which is equal to $20 \mu\text{A}$ for (A)–(C) and $50 \mu\text{A}$ for (D)–(F). Scans began and ended at the vertical mark. $E_{1/2}$ was determined in a region of reversible kinetics and is reported vs. the onset of solvated electrons.

TABLE 2

Cyclic voltammetric results and rate constants for the first reduction and irreversible dimerization of quinoline in ammonia + $\text{CF}_3\text{SO}_3\text{K}$ at low temperature. See text for explanation of symbols

$v/\text{V s}^{-1}$	$i_{p,c}v^{-1/2}c_Q^{-1}/\mu\text{A s}^{1/2}\text{V}^{-1/2}\text{M}^{-1}$	$i_{p,a}/i_{p,c}$	τ/s	$10^{-2}k_2/\text{M}^{-1}\text{s}^{-1}$
$T = -70^\circ\text{C}$, $c_Q = 5.67 \text{ mM}$				
0.10	8.5	0.55	1.17	3.7
0.20	8.2	0.53	1.06	3.2
0.50	7.4	0.70	0.312	5.0
1.00	7.3	0.80	0.145	4.7
2.00	6.6	0.86	0.082	4.9
				Avg. = 4.3 ± 0.8
$T = -40^\circ\text{C}$, $c_Q = 5.59 \text{ mM}$				
0.20	11.7	0.54	0.565	9.4
0.50	11.0	0.65	0.218	11.0
1.00	10.3	0.72	0.133	10.8
2.00	9.84	0.82	0.0645	10.7
				Avg. = 10.5 ± 0.7

TABLE 3

Cyclic voltammetric results for first reductions of quinoline and acridine at high temperature. See text for explanation of symbols

<i>Quinoline</i>		20 °C		40 °C		70 °C		100 °C	
		<i>P</i> = 8.1 bar		14 bar		34 bar		61 bar	
		<i>c_Q</i> = 4.77 mM		4.57 mM		4.01 mM		3.65 mM	
<i>v/V s⁻¹</i>	$\frac{i_{p,a}/i_{p,c}}{i_{fun}/\mu A s^{1/2}}$ $V^{-1/2} M^{-1}$	$\frac{i_{p,a}/i_{p,c}}{i_{fun}/\mu A s^{1/2}}$ $V^{-1/2} M^{-1}$	$\frac{i_{p,a}/i_{p,c}}{i_{fun}/\mu A s^{1/2}}$ $V^{-1/2} M^{-1}$	$\frac{i_{p,a}/i_{p,c}}{i_{fun}/\mu A s^{1/2}}$ $V^{-1/2} M^{-1}$	$\frac{i_{p,a}/i_{p,c}}{i_{fun}/\mu A s^{1/2}}$ $V^{-1/2} M^{-1}$	$\frac{i_{p,a}/i_{p,c}}{i_{fun}/\mu A s^{1/2}}$ $V^{-1/2} M^{-1}$	$\frac{i_{p,a}/i_{p,c}}{i_{fun}/\mu A s^{1/2}}$ $V^{-1/2} M^{-1}$	$\frac{i_{p,a}/i_{p,c}}{i_{fun}/\mu A s^{1/2}}$ $V^{-1/2} M^{-1}$	$\frac{i_{p,a}/i_{p,c}}{i_{fun}/\mu A s^{1/2}}$ $V^{-1/2} M^{-1}$
0.20	0.74	17	0.92	22				0.84	26
0.50	0.73	15	0.94	20	0.91	26		0.90	24
1.00	0.75	15	0.91	19	0.97	25		0.96	24
2.00	0.71	15	0.89	19	0.98	24		0.96	23
4.00	0.70	15	0.87	18	1.00	23		0.99	23
6.00	0.72	15	0.84	17	1.00	23		0.99	22
8.00	0.76	15			0.99	23		1.01	22
10.0	0.81	15			0.99	213		1.01	22
15.0					1.01	23			
20.0	0.86	15							
50.0	0.94	15							
<i>Acridine</i>		20 °C		50 °C		100 °C		150 °C	
		<i>P</i> = 8.1 bar		19 bar		61 bar		300 bar	
		<i>c_A</i> = 6.14 mM		5.76 mM		4.70 mM		4.30 mM	
<i>v/V s⁻¹</i>	$\frac{i_{p,a}/i_{p,c}}{i_{fun}/\mu A s^{1/2}}$ $V^{-1/2} M^{-1}$	$\frac{i_{p,a}/i_{p,c}}{i_{fun}/\mu A s^{1/2}}$ $V^{-1/2} M^{-1}$	$\frac{i_{p,a}/i_{p,c}}{i_{fun}/\mu A s^{1/2}}$ $V^{-1/2} M^{-1}$	$\frac{i_{p,a}/i_{p,c}}{i_{fun}/\mu A s^{1/2}}$ $V^{-1/2} M^{-1}$	$\frac{i_{p,a}/i_{p,c}}{i_{fun}/\mu A s^{1/2}}$ $V^{-1/2} M^{-1}$	$\frac{i_{p,a}/i_{p,c}}{i_{fun}/\mu A s^{1/2}}$ $V^{-1/2} M^{-1}$	$\frac{i_{p,a}/i_{p,c}}{i_{fun}/\mu A s^{1/2}}$ $V^{-1/2} M^{-1}$	$\frac{i_{p,a}/i_{p,c}}{i_{fun}/\mu A s^{1/2}}$ $V^{-1/2} M^{-1}$	$\frac{i_{p,a}/i_{p,c}}{i_{fun}/\mu A s^{1/2}}$ $V^{-1/2} M^{-1}$
0.50	0.70	17	0.91	18	0.94	20		0.93	22
1.00	0.65	16	0.89	18	0.98	17		0.99	21
2.00	0.59	16	0.86	17	1.00	16		1.02	21
4.00	0.55	16	0.79	17	0.99	16		1.04	20
6.00	0.56	15	0.76	17	1.01	16		1.05	19
8.00	0.54	15	0.75	17	1.03	16		1.04	19
10.0	0.54	15	0.74	17	1.02	15		1.06	19
12.0	0.54	14	0.73	17	1.01	15		1.05	18
20.0	0.41	13	0.72	16	1.01	15			
50.0	0.56	12							

The low value in the second case [6b] may have been due to the presence of a trace of water in the system. In general, water will act to increase the speed of the dimerization [17]; however, partial passivation of the electrode by precipitated KOH would suppress k_2 . Additionally, the diffusion coefficient (D), which corresponds to the reported k_2 ($D = 8.2 \times 10^{-6} \text{ cm}^2 \text{ s}^{-1}$), is much lower than the one found in this study ($D = 2.7 \times 10^{-5} \text{ cm}^2 \text{ s}^{-1}$) or for similar molecules in ammonia at -40°C [1b,6a,7a]. If the error in D is assumed to have arisen through the concentration, or a smaller electrode area because of partial passivation by KOH, and the rate is recalculated based on a lower concentration estimated from the differences in the

diffusion coefficients, k_2 is equal to $1.2 \times 10^3 \text{ M}^{-1} \text{ s}^{-1}$, which is close to the value we report.

The dimerization reaction of $\text{Q}^{\cdot-}$ displays some degree of reversibility as the temperature is raised, Fig. 4c. In this temperature domain, a plot of $i_{p,a}$ vs. v should display a minimum, if a reversible DIM1 process occurs. At very fast scan rates (zone DO), $i_{p,a}/i_{p,c} = 1$, and at slow scan rates (zone DE or DI), $i_{p,a}/i_{p,c} = 1$. However, at intermediate values of v , $i_{p,a}/i_{p,c} < 1$, since the kinetics are reasonably facile in either direction. We detected this behavior between -30 and 60°C with the range of scan rates available ($v = 0.2\text{--}50 \text{ V s}^{-1}$), Table 3. This observation precludes a significant contribution from an irreversible DIM2 process, because for any totally irreversible reaction (EC_i), $i_{p,a}/i_{p,c}$ can only increase with v . At 20°C , the change in i_{fun} with the kinetic parameter $\lambda^{1/2}\chi^{3/4}$, Table 3, is small and follows the trend expected for a reversible DIM1 reaction [14f]. Similar results are found at 40°C ; however, at slower scan rates, interference from convection appears to inflate the current function.

Above 60°C , Figs. 4d,e, the kinetics become so facile in both directions that $i_{p,a}/i_{p,c} \cong 1$, except at the slowest scan rates, where convection probably interferes in the measurement. Near 125°C , the first reduction wave is too close to the second reduction for reliable measurements of $i_{p,a}/i_{p,c}$, Fig. 4f.

In the absence of K^+ (i.e., with TBA^+ as supporting electrolyte cation), no dimeric species were detected at any v at room temperature; and the voltammetric analysis indicated a reversible electron transfer with formation of a stable product on the voltammetric time scale (zone DO), Fig. 5. At -40°C , $\text{CF}_3\text{SO}_3\text{TBA}$ was relatively insoluble in ammonia; but by using an ultramicroelectrode, we detected a reduced plateau current upon scan reversal, suggesting very slow dimerization. We estimate that the magnitude of k_2 falls by about two orders in the absence of K^+ . No measurements were made above 22°C , because $\text{CF}_3\text{SO}_3\text{TBA}$ is unstable in ammonia at elevated temperature.

The cyclic voltammetry at various temperatures for potentials encompassing both reduction waves of Q is shown in Fig. 6. The voltammetry is somewhat difficult to analyze because of the proximity of the second wave to the onset of e_s^- , but several features are evident. At low temperature, the height of the second wave is smaller than expected for a second one-electron process (eqn. 3). This is consistent with the dianion–substrate coupling mechanism DIM3, because Q^{2-} reacts with Q as it diffuses away from the electrode surface, the concentration of Q falls, and the height of the second wave is suppressed. The dimerization of $\text{Q}^{\cdot-}$ (eqn. 2) also removes a portion of the contribution to the current at the second wave from $\text{Q}^{\cdot-}$.

Close examination of Figs. 6A–C reveals a very small anodic current at a potential corresponding to the oxidation of Q_2^{2-} . It is interesting that a wave corresponding to the oxidation Q_2^{2-} is detectable at room temperature, when the scan is continued past the potential for the second reduction of Q (Fig. 6c), while the wave is not detectable if the potential is reversed prior to the second reduction (Fig. 4c), since the kinetics of the monomerization must be the same in either case. Probably e_s^- formed coincidentally with the second wave promotes formation of

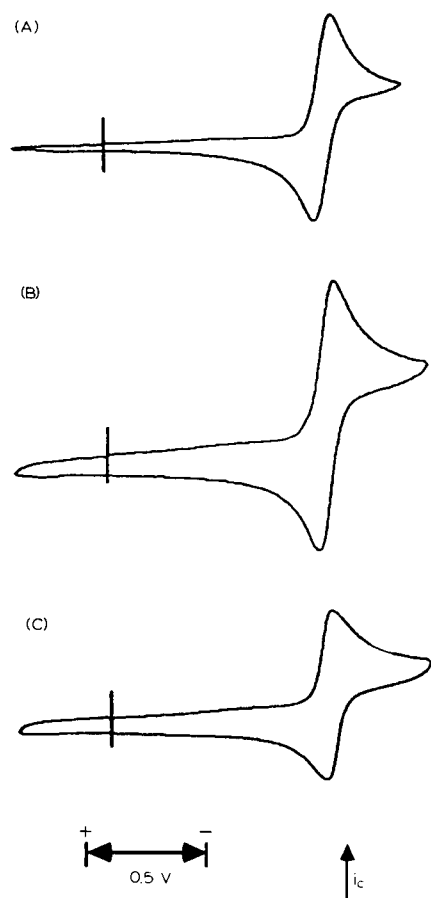


Fig. 5. Cyclic voltammetry of the first reduction of quinoline (Q) at various scan rates in ammonia + $\text{CF}_3\text{SO}_3\text{TBA}$ at 22°C and 300 bar. For scan rates between 0.1 and 500 V s^{-1} , $i_{p,a}/i_{p,c} = 1.0 \pm 0.04$, and $\Delta E_p = 70 \pm 10\text{ mV}$. The height of the vertical mark on each voltammogram represents the current scale (i_{sc}), and the initial and final potentials. For $v \leq 1.0\text{ V s}^{-1}$ the electrode area (A) was $2.9 \times 10^{-3}\text{ cm}^2$, and for higher scan rates $A = 1.2 \times 10^{-4}\text{ cm}^2$. $[\text{Q}] = 9.17\text{ mM}$, $[\text{CF}_3\text{SO}_3\text{TBA}] = 0.18\text{ M}$. TBA is the tetra-*n*-butylammonium cation. All potentials are vs. e_s^- . (A) $v = 1.0\text{ V s}^{-1}$, $i_{sc} = 25\text{ }\mu\text{A}$, $i_{p,a}/i_{p,c} = 1.00$, $i_{p,c}v^{-1/2}A^{-1} = 19.5\text{ mA s}^{1/2}\text{ V}^{-1/2}\text{ cm}^{-2}$, $E_{1/2} = +0.635\text{ V}$, $\Delta E_p = 70\text{ mV}$; (B) $v = 10\text{ V s}^{-1}$, $i_{sc} = 2.5\text{ }\mu\text{A}$, $i_{p,a}/i_{p,c} = 0.99$, $i_{p,c}v^{-1/2}A^{-1} = 20.2\text{ mA s}^{1/2}\text{ V}^{-1/2}\text{ cm}^{-2}$, $E_{1/2} = +0.641\text{ V}$, $\Delta E_p = 60\text{ mV}$; (C) $v = 100\text{ V s}^{-1}$, $i_{sc} = 25\text{ }\mu\text{A}$, $i_{p,a}/i_{p,c} = 0.97$, $i_{p,c}v^{-1/2}A^{-1} = 19.5\text{ mA s}^{1/2}\text{ V}^{-1/2}\text{ cm}^{-2}$, $E_{1/2} = +0.635\text{ V}$, $\Delta E_p = 60\text{ mV}$.

additional dimer. This was verified by scans deep into the e_s^- background and noting that the primary product was dimer rather than monomer. At higher temperatures the reverse kinetics become so facile that the dimer is not observed on the voltammetric time scale, Figs. 6D–F, and the second wave is roughly the same height as the first. This result, along with the absence of a reversal current at the

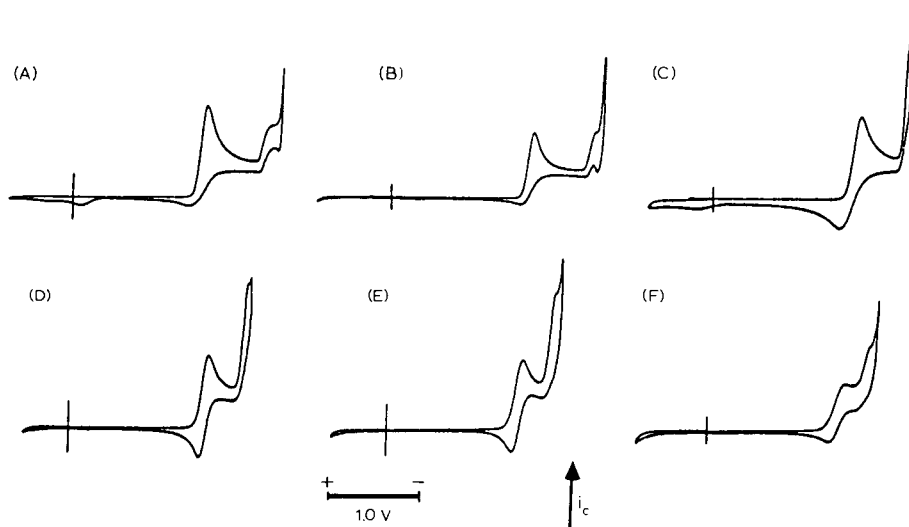


Fig. 6. Cyclic voltammetry of the first two reductions of quinoline in ammonia + $\text{CF}_3\text{SO}_3\text{K}$. Conditions for (A)–(F) are the same as in Fig. 4.

second wave, is consistent with a DIM3 reaction in fast equilibrium with the anion radical in the reaction layer:



Note that in Fig. 6 the two reduction waves move toward each other as the temperature is raised; i.e., the cathodic peak separation ($\Delta E_{p,c}$) decreases. This behavior is the same as that found for A, but contrary to our previously reported results for structurally related compounds [1b]. This subject will be discussed in more detail later.

The voltammetry for the first reduction of A, Fig. 7, suggests a follow-up dimerization in the presence of K^+ similar to that found for Q. Even at -40°C no reverse wave is observed at scan rates up to 50 V s^{-1} , indicating that k_2 is larger than for Q, but k_{-2} does not increase proportionally; that is, K_2 is larger for A than for Q at any temperature. At -65 and -40°C , the current function decreased with scan rate between 18 and 22%, Table 2, and the changes of $E_{p,c}$ with $\log v$ were also near the theoretical values for a totally irreversible DIM1 reaction.

In the intermediate temperature range, 0 to 60°C , the voltammetry indicates an equilibrium between dimer and monomer, and a minimum appears in a plot of $i_{p,a}/i_{p,c}$ vs. v (Table 3), as was the case for the quinoline system at moderate temperature. The i_{lim} data listed in Table 3 also support a reversible DIM1 scheme.

Above 60°C , the voltammetric data, Table 3, indicate reversible electrochemistry with stable product. It was not possible to make meaningful estimates of $\partial E_{p,c}/\partial \log$

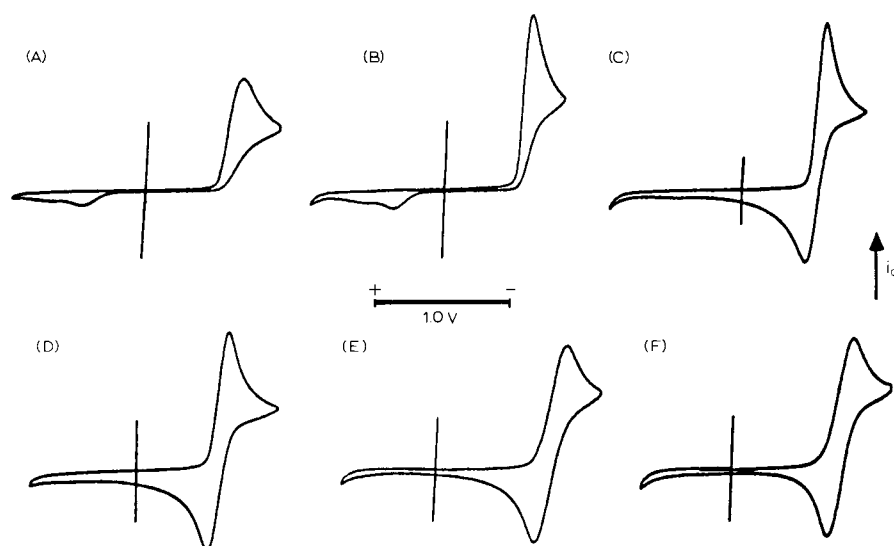


Fig. 7. Cyclic voltammetry of the first reduction of acridine (A) in ammonia + $\text{CF}_3\text{SO}_3\text{K}$ at a tungsten working electrode ($A = 0.0083 \text{ cm}^2$) between -65 and 150°C . (A) $T = -65^\circ\text{C}$, $P = 0.10 \text{ bar}$, $[\text{A}] = 7.24 \text{ mM}$, $E_{1/2} = +1.270 \text{ V}$, $v = 0.20 \text{ V s}^{-1}$; (B) $T = -40^\circ\text{C}$, $P = 0.70 \text{ bar}$, $[\text{A}] = 6.94 \text{ mM}$, $E_{1/2} = +1.136 \text{ V}$, $v = 0.20 \text{ V s}^{-1}$; (C) $T = 20^\circ\text{C}$, $P = 8.1 \text{ bar}$, $[\text{A}] = 6.14 \text{ mM}$, $E_{1/2} = +1.023 \text{ V}$, $v = 0.20 \text{ V s}^{-1}$; (D) $T = 50^\circ\text{C}$, $P = 19 \text{ bar}$, $[\text{A}] = 5.65 \text{ mM}$, $E_p = +1.000 \text{ V}$, $v = 1.0 \text{ V s}^{-1}$; (E) $T = 100^\circ\text{C}$, $P = 61 \text{ bar}$, $[\text{A}] = 4.70 \text{ mM}$, $E_p = +1.015 \text{ V}$, $v = 1.0 \text{ V s}^{-1}$; (F) $T = 150^\circ\text{C}$, $P = 300 \text{ bar}$, $[\text{A}] = 4.30 \text{ mM}$, $E_{1/2} = +0.848 \text{ V}$, $v = 1.0 \text{ V s}^{-1}$. The concentration of $\text{CF}_3\text{SO}_3\text{K}$ was 0.20 M at -65°C , and fell to 0.12 M at 150°C because of the decrease in solvent density. The current scale is indicated by the height of the vertical mark on each figure which is equal to $20 \mu\text{A}$ for (A)–(C) and $75 \mu\text{A}$ for (D)–(F). Scans began and ended at the vertical mark. $E_{1/2}$ was determined in a region of reversible kinetics and is reported vs. the onset of solvated electrons. Potentials are vs. e_3^- .

v at higher temperatures because of errors in the measured potential introduced by the high solution resistance. It is likely, however, that the system is near the middle of the KG zone at the higher temperatures. This is suggested by the elevated current ratios found at 100 and 150°C , Table 3. In certain instances, $i_{p,a}/i_{p,c}$ can exceed 1 for a reversible dimerization reaction [20]. In effect, some of $\text{R}^{\cdot-}$ is stored as R_2^{2-} , and when the potential is stepped positive, some of the dimer near the electrode surface dissociates, creating an excess of $\text{R}^{\cdot-}$. For DPSC, it can be shown that this situation occurs in zone KG.

Figure 8 shows the voltammetry encompassing the first two reduction waves of A. Although the behavior is similar to that previously described for Q, there are significant differences at the lowest temperatures. Particularly noticeable is the absence of a wave corresponding to the second reduction of A, Figs. 8A,B. This feature is rather difficult to rationalize, since it implies that either $\text{A}^{\cdot-}$ cannot be reduced at low temperature or that it is reduced, but is so unstable kinetically that it reacts quickly to produce a species that transfers an electron back to the electrode.

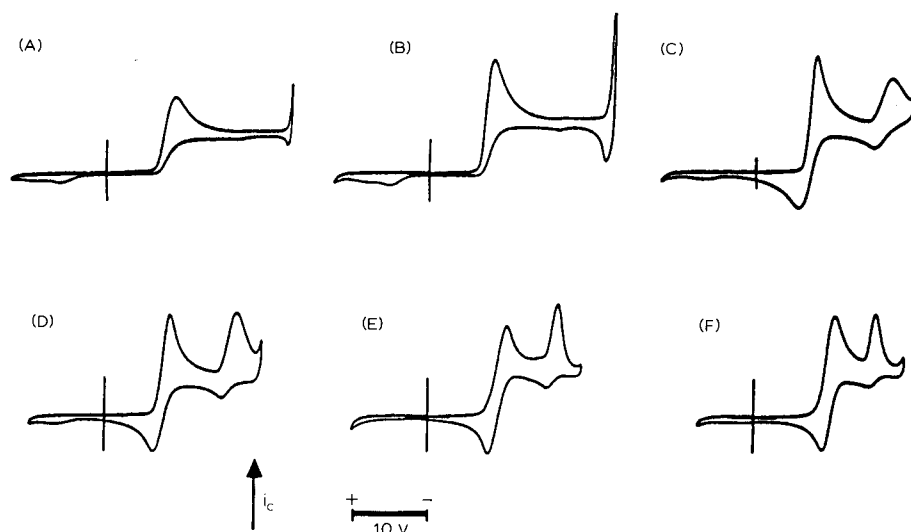


Fig. 8. Cyclic voltammetry of the first two reductions of acridine in ammonia + $\text{CF}_3\text{SO}_3\text{K}$. Conditions for (A)–(F) are the same as Fig. 7. E_p for the second waves are: (C) +0.250 V; (D) +0.383 V; (E) +0.476 V; (F) +0.441 V.

The latter situation seems unlikely, since reasonable products are probably those of DIM1 or DIM3. Neither of these would transfer an electron back to the electrode spontaneously at so negative a potential; thus the second electron transfer must be inhibited at low temperature. This subject is discussed in more detail later.

At room temperature and above, Fig. 8C–F, the electrochemistry of the second reduction is qualitatively similar to that of Q; the magnitude of the second wave is suppressed; upon scan reversal, little or no backwave is found for A^{2-} ; and $\Delta E_{p,c}$ decreases with temperature. These points are consistent with a DIM3 process in rapid equilibrium with the anion radical, eqns. (8) and (9).

The polarographic half-wave potentials ($E_{1/2}$) for the first reductions of A and Q, determined from the cyclic voltammetric $E_{p,c}$ values, are plotted as solid points in Fig. 9. The points corresponding to $E_{p,c}$ for A at high temperature (open squares) were not included for reasons given previously. The line drawn through the corrected $E_{1/2}$ values yield slopes ($dE_{1/2}/dT$) of -2.6 and -2.0 $\text{mV}/^\circ\text{C}$ for the first reductions of A and Q, respectively. These values are in good agreement with those found previously for the first and second reductions of the diaza-aromatics where the average slope was -2.4 $\text{mV}/^\circ\text{C}$ [1b]. This implies that the entropy of formation for radical anions of aromatic species in ammonia is ca. -230 $\text{J}/\text{mol K}$. Note that all potentials were measured versus the potential of the solvated electron in ammonia, e_s^- , so the entropy we have measured is for the reaction



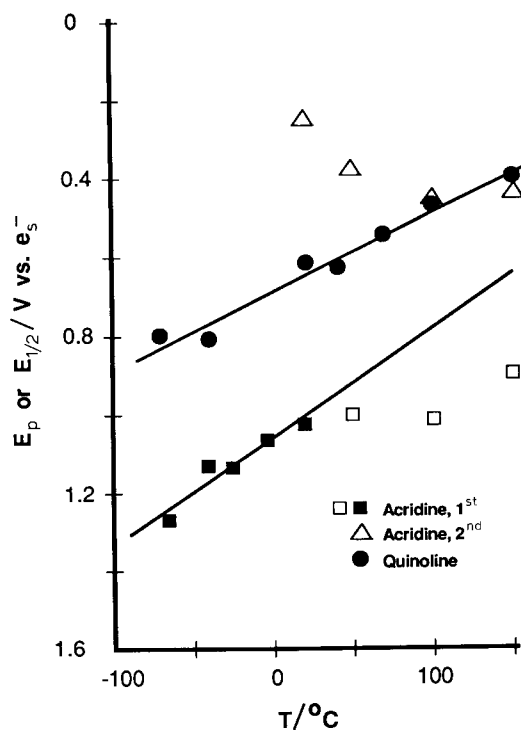


Fig. 9. Dependence of the polarographic half-wave potential ($E_{1/2}$) or peak potential (E_p) on temperature for the first reduction of Q, and the first and second reductions of A. The slopes of the lines (dE/dT) are: A, $-2.6 \text{ mV}/^\circ\text{C}$; Q, $-2.0 \text{ mV}/^\circ\text{C}$. The closed circles and squares are $E_{1/2}$ values corrected for kinetics, and the open triangles and squares are E_p not corrected for kinetics.

The entropy of eqn. (10) can be converted into that of eqn. (11)



if the entropy for ammoniacal solvation of the electron is known [1b].

The variation of $E_{p,c}$ with temperature for the second reduction of A, E_{p2A} , is plotted in Fig. 9 as open triangles. The peak potentials for the second reduction of Q are not shown, since the wave was too close to the background for reliable measurement. However, qualitatively $\Delta E_{p,c}$ for Q followed the same trend found for A. At the lowest temperature no wave is found for the second reduction of A, but as the temperature is raised, a wave is observed, and $E_{p,c}$ shifts positive; that is, E_{p2} shifts closer to the first wave. This observation is contrary to that found for the second reductions of quinoxaline and phenazine (which resulted in stable dianions), where $dE_{1/2}/dT$ for the second reductions was linear and equal to ca. $-2.4 \text{ mV}/^\circ\text{C}$. The deviation in the present case probably arises from the complicating

TABLE 4

Kinetic and thermodynamic parameters for the acridine and quinoline systems

$T/^{\circ}\text{C}$	P/bar	Conc./mM	$k_2/M^{-1}\text{ s}^{-1}$	k_{-2}/s^{-1}	K_2/M^{-1}
<i>Acridine</i>					
22	8.1	6.14	2.8×10^5	17.5	1.6×10^4
-5	3.5	6.50	1.3×10^5	2.7	4.9×10^4
-15	2.3	6.63	9.5×10^4	0.63	1.5×10^5
-27	1.4	6.80	7.4×10^4	0.080	9.2×10^5
<i>Quinoline</i>					
21	8.1	7.44	4.8×10^3	5.7	8.4×10^2
22	300	9.27	3.8×10^3	3.9	9.6×10^2
0	4.2	8.00	3.3×10^3	0.66	5.0×10^3
-11	2.7	5.14	1.9×10^3	0.31	6.2×10^3
-40 ^a	0.7	5.59	1.1×10^3		
-70 ^a	0.1	5.67	4.3×10^2		

^a At these temperatures k_{-2} and K_2 were not obtained.

dimerization reaction. In the absence of other reactions, $\Delta E_{p,c}$ is related to the equilibrium constant for the synproportionation reaction:



$$K_{\text{SYN}} = [\text{Q}^{\cdot-}]^2 / ([\text{Q}^{2-}][\text{Q}]) \quad (13)$$

$$\Delta E_{p,c} = (RT/nF) \ln K_{\text{SYN}} \quad (14)$$

In the present case, especially at low temperature, the DIM3 reaction operates parallel to, and probably dominates, the synproportionation, eqn. (12). In the next section, it will be shown that K_2 , the DIM1 equilibrium constant, decreases with increasing temperature (Table 4). Since the dimer formed by either DIM1 or DIM3 is the same, it is reasonable to expect a similar temperature dependency for DIM3. Therefore, at low temperature the equilibrium controlling the positions of the second waves is probably a complex function of K_{SYN} and K_{DIM3} , the equilibrium constant for the DIM3 reaction. At 150°C the effect of the dimerization is less important, and E_{p2A} begins to shift in the negative direction. This suggests that when the dimerization reaction is not significant, the synproportionation dominates the overall equilibrium and behavior similar to that found for the uncomplicated second electron transfers of phenazine and quinoxaline is manifested in the voltammetry of A. If a line is drawn between the three lowest temperature points plotted for the second reduction of A, Fig. 9, and extrapolated to lower temperatures, E_{p2A} is predicted to lie well within the background process at -70°C and just negative of 0 V at -40°C. Close examination of Fig. 8B reveals a slight broadening of the current related to the generation of e_s^- and a broadening of the corresponding oxidation wave. These deformations may be due to the second reduction and oxidation of A. A detailed explanation of the thermodynamics and kinetics of this second process is beyond the scope of this work.

Double potential step chronoamperometry

In the intermediate temperature region, it was possible to quantify the rate of the reversible dimerization of $Q^{\cdot-}$ and $A^{\cdot-}$ using the DPSC technique. Figure 10 presents the data in the form of plots of R vs. $\log \theta$ at temperatures between -27 and 22°C . The reproducibility of these plots was verified using different concentrations of substrate in separate experiments. A slight difference in K_2 over the pressure range 8 to 300 bar, Table 4, may indicate that the dimer is favored at higher pressure; that is, the change in reaction volume may favor the dimer. However, the magnitude of the observed difference in K_2 is close to the expected accuracy of the measurement. Perhaps the dielectric constant of the medium (which

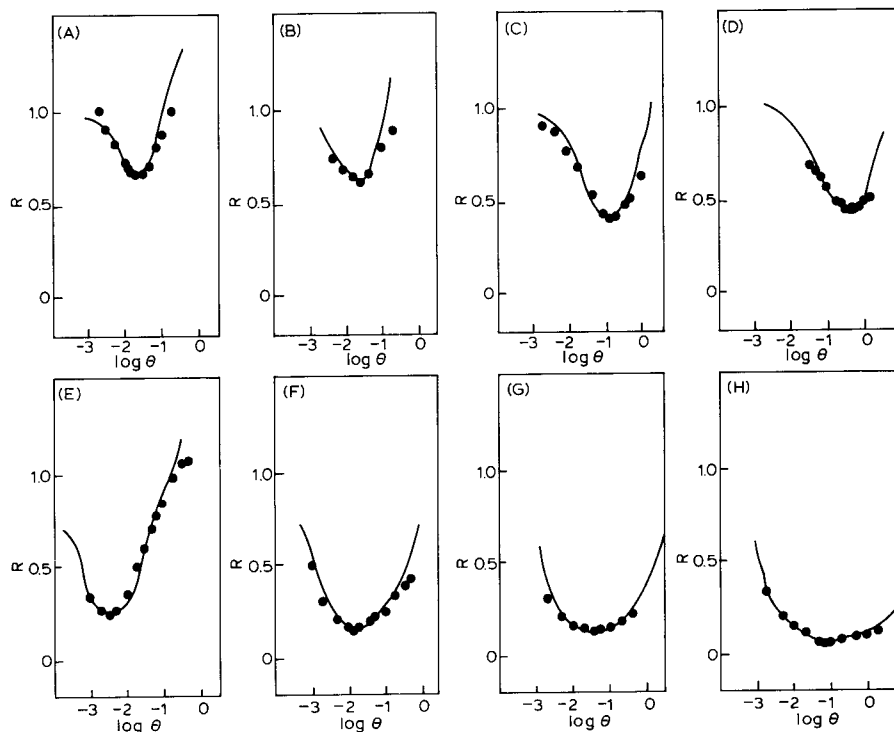


Fig. 10. Double potential step chronoamperometric analysis of the electro-dimerization of Q (A)–(D) and A (E)–(H) in ammonia containing 0.14 to 0.20 M $\text{CF}_3\text{SO}_3\text{K}$. θ is the potential reversal time in seconds, and R is the normalized current ratio. The lines connecting the experimentally determined points were derived from a working curve [20]. (A) $T = 21^\circ\text{C}$, $P = 8.1$ bar, $[\text{Q}] = 7.44$ mM , $K_2 = 8.4 \times 10^2 M^{-1}$; (B) $T = 22^\circ\text{C}$, $P = 300$ bar, $[\text{Q}] = 9.27$ mM , $K_2 = 9.6 \times 10^2 M^{-1}$; (C) $T = 0^\circ\text{C}$, $P = 4.2$ bar, $[\text{Q}] = 8.00$ mM , $K_2 = 5.0 \times 10^3 M^{-1}$; (D) $T = -11^\circ\text{C}$, $P = 2.7$ bar, $[\text{Q}] = 5.14$ mM , $K_2 = 6.2 \times 10^3 M^{-1}$; (E) $T = 22^\circ\text{C}$, $P = 8.1$ bar, $[\text{A}] = 6.14$ mM , $K_2 = 1.6 \times 10^4 M^{-1}$; (F) $T = -5^\circ\text{C}$, $P = 3.5$ bar, $[\text{A}] = 6.50$ mM , $K_2 = 4.9 \times 10^4 M^{-1}$; (G) $T = -15^\circ\text{C}$, $P = 2.3$ bar, $[\text{A}] = 6.63$ mM , $K_2 = 1.5 \times 10^5 M^{-1}$; (H) $T = -27^\circ\text{C}$, $P = 1.4$ bar, $[\text{A}] = 6.80$ mM , $K_2 = 9.2 \times 10^5 M^{-1}$.

increases with pressure) favors the anion radical, partially compensating the effects of reaction volume. In any case, the compressibility of liquid ammonia is not great, and large changes in K_2 with P are not expected below T_c .

It would be of interest to make measurements of dK_2/dP in the critical region where the advantage of the large compressibility of the SCF could be used to draw conclusions regarding the reaction volume of the dimer and monomer. Such measurements were not made for this system, because it was not possible to collect equilibrium data at temperatures significantly above room temperature, as the minima of the R vs. $\log \theta$ plots fell in an inaccessible time domain. The plots of Fig. 10 were fitted to the working curves (ref. 20, Figs. 1, 8) to obtain values of k_2 , k_{-2} , and K_2 . The results are shown in Table 4. The trend is exactly that expected from the voltammetry; K_2 decreases with increasing temperature, reflecting an increase in k_{-2} relative to k_2 .

The Arrhenius plots, Fig. 11, derived from the DPSC and voltammetric data are linear and lead to: $E_{a,Q2} = 12$, $E_{a,Q-2} = 55$, $E_{a,A2} = 17$ and $E_{a,A-2} = 65$ kJ mol⁻¹ for the forward and backward activation energies of Q^{•-} and A^{•-}, respectively. The corresponding pre-exponential factors for the forward dimerizations of Q^{•-} and A^{•-} are: $A_{Q2} = 7 \times 10^5$ and $A_{A2} = 3 \times 10^8$ M⁻¹ s⁻¹. These values are close to those found for 9-cyanoanthracene (ANCN) [19]: $E_{a,ANCN2} = 19.2$, $E_{a,ANCN-2} = 72.8$ kJ mol⁻¹ and $A_{ANCN2} = 7.9 \times 10^8$ M⁻¹ s⁻¹. The latter value is in excellent agreement with the three ring aza-analog (A), but higher than the corresponding value for Q. This is surprising, since presumably the pre-exponential is reduced because of steric hindrance and the delocalization of the excess electron over the ring [19,23]. Based on these two considerations, Q should have a larger pre-exponential factor than A. Perhaps specific mechanistic or symmetry factors are responsible for this observation.

Other examples of the Arrhenius pre-exponential factor dominating the kinetics of dimerization reactions have been reported. For example, the dimerization of the tri-*t*-butylcycloheptatrienyl radical has a relatively low activation energy ($E_a = 8.0$ kJ mol⁻¹), but the rate constant is only 3×10^5 M⁻¹ s⁻¹ at 22°C [24]. The rate for the irreversible dimerization of pyridine at -40°C in the presence of K⁺ has been reported as $(1.5-4.0) \times 10^5$ M⁻¹ s⁻¹ in ammonia [7a], which is somewhat faster than we would predict for A under the same conditions based on the Arrhenius plot, Fig. 11B. Measurements of k_2 for pyridine were not made at other temperatures, and therefore the values of E_a and A cannot be compared. k_2 has been given as $(8 \pm 5) \times 10^5$ M⁻¹ s⁻¹ for pyrimidine in AN at room temperature [7c], which is also close to that found for A at 22°C in ammonia.

The Arrhenius plots were extrapolated to obtain predicted values for k_2 and k_{-2} over the temperature range -70 to +150°C. This allowed calculation of the dimensionless parameters $\chi = 1/K_2 c_R^*$ and $\lambda = (RT/F)(k_2 c_R^*/v)$ throughout the temperature range studied. The resulting values were overlaid on the kinetic zone diagram, Fig. 2, to determine the agreement between the DPSC measurements and the cyclic voltammetry and to determine if the extrapolation of kinetic data into the supercritical regime is justified. The points plotted on Fig. 2 correspond to the

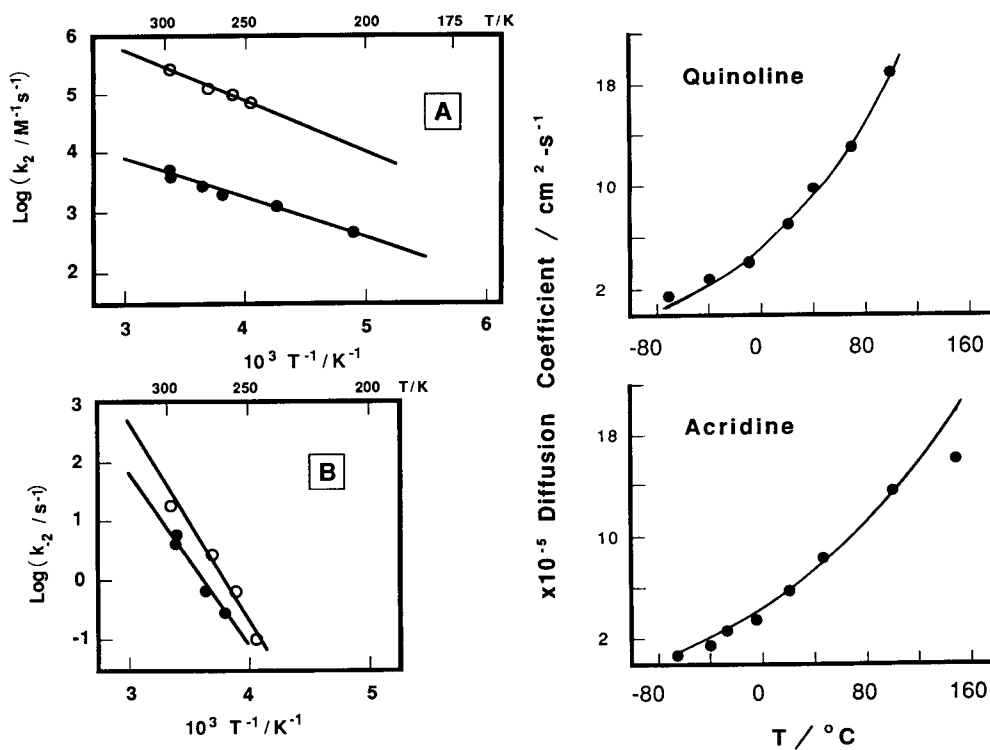


Fig. 11. Arrhenius plots for the electrodimers of Q (●) and A (○) in ammonia containing 0.14 to 0.20 M $\text{CF}_3\text{SO}_3\text{K}$. (A) Forward dimerization rate constant, k_2 . $E_{a,Q} = 12 \text{ kJ/mol}$; $A_{Q,2} = 7 \times 10^5 \text{ M}^{-1} \text{ s}^{-1}$; $E_{a,A} = 17 \text{ kJ/mol}$; $A_{A,2} = 3 \times 10^8 \text{ M}^{-1} \text{ s}^{-1}$. (B) Backward dimerization rate constant, k_{-2} . $E_{a,Q} = 55 \text{ kJ/mol}$; $A_{Q,-2} = 1 \times 10^{10} \text{ s}^{-1}$; $E_{a,A} = 65 \text{ kJ/mol}$; $A_{A,-2} = 8 \times 10^{12} \text{ s}^{-1}$.

Fig. 12. Dependence of the diffusion coefficients on temperature. The points represent the experimental data, and the solid line represents the Stokes-Einstein fit based on the experimentally determined effective molecular radius (r) at 25°C : Q, $r = 0.227 \text{ nm}$; A, $r = 0.293 \text{ nm}$.

voltammetry displayed in Figs. 4 and 7 for Q and A, respectively. That is, the values for c_R^* and temperature, required for calculation of χ and λ , were the same as in the voltammograms. The scan rate used for calculation of the points in Fig. 2 was 1 V s^{-1} . For A, the agreement between the extrapolated kinetic data and the voltammetry of Fig. 7 is excellent. For example, the third point up from the bottom of Fig. 2 on line A corresponds to Fig. 7C at 1 V s^{-1} . Under these conditions, the state of the system is predicted to correspond to zone KE. This is a particularly sensitive region of the zone diagram, since relatively small variations of v can switch the voltammetry into KP or KO. Examination of the data in Table 3 for A at 20°C indicates that the behavior predicted by the extrapolated DPSC data is found experimentally. The current ratio, $i_{p,a}/i_{p,c}$, increases with decreasing scan rate (corresponding to an increase in λ) as the system moves farther from the totally irreversible behavior

found in zone KP toward zone KO. At 20 V s^{-1} , the current ratio is at a minimum, and by 50 V s^{-1} , it again increases as zone KO is approached.

Similar behavior is observed at higher temperature, particularly at 150°C where the current ratio exceeds 1, reaching a maximum of 1.06 at $v = 12 \text{ V s}^{-1}$, Table 2. Under these conditions the state of the reaction must be in zone KG, in agreement with the extrapolated DPSC data. An analysis of the correspondence between the voltammetry and extrapolated DPSC kinetic data of Q results in similar agreement.

The resultant behavior suggests that by adjustment of temperature, the state of the DIM1 reaction can be moved vertically along the χ axis relatively independently of λ . Then, by choosing λ through adjustment of v (or θ), any zone can be addressed. This temperature dependent system could be used to select among competitive pathways for electro-organic syntheses or to verify a proposed mechanism.

Diffusion coefficients

A plot of the diffusion coefficient (D) versus temperature for Q and A is shown in Fig. 12. Over the range of temperatures studied, D increases by an order of magnitude, in agreement with previous results [1b]. A one-electron reduction per equivalent of both Q and A was assumed for the calculation of D , and the excellent agreement obtained with previous results provides additional evidence for the predominance of either the DIM1 or single-wave DIM2 mechanism.

The experimentally determined diffusion coefficients shown in Fig. 12 are correlated by a curve which represents the predicted diffusion coefficients based on the Stokes–Einstein equation and the experimentally determined effective molecular radius at 25°C [1b]. The fit is quite good, and is in agreement with that found previously, suggesting that near-critical and supercritical fluids adhere to general theoretical models for solvents.

CONCLUSIONS

We have shown that the dimerization reactions of the radical anions of Q and A follow the DIM1 reaction mechanism. At low temperature, this reaction can be considered irreversible, but the back reaction must be considered at higher temperatures. Additionally, we have demonstrated that large temperature excursions (220°C) can be used to tune the nature and rate of chemical reactions in a predictable way. The supercritical state appears as a simple extension of the liquid state, in that no dramatic differences are found in rates or products when the critical temperature of the solvent is exceeded. This result is important because it means that the unique characteristics of the supercritical state (tunable dielectric constant, density, compressibility, etc.) can be exploited independently of other complicating factors. For example, the highly compressible supercritical state could be used to adjust the equilibrium constant of electrochemically initiated homogeneous reactions involving large changes in reaction volume. The dielectric constant of the supercritical fluid

(SCF) can be varied with pressure to select preferentially (by lowering E_a) reaction mechanisms that have a strong dependence on the dielectric constant of the transition state.

As was found previously [1b], the radical anions displayed stability, even at 150°C in the SCF. However, the dianion of A is not stable on the voltammetric time scale and probably forms a dimer through the DIM3 mechanism. The activation energies for the DIM1 process are similar to those found for other radical anions in a number of different solvents, and while the collision frequencies are lower than those predicted by theory, they are in line with experimentally determined values for related species. The equilibrium concentrations of dimeric dianions have been correlated to the dielectric constant of the solvent [6a], but we have shown that temperature plays a far more important role. The equilibrium concentration of dimer was found to fall dramatically with increasing temperature even though the dielectric constant of ammonia also falls by an order of magnitude in the temperature range used for these experiments.

In conjunction with the previous study [1b], we have shown that the Stokes–Einstein relation for diffusion is generally applicable to supercritical fluids. The entropy of the reaction between e_s^- and Q and A to form the radical anions was found to be in agreement with previous results. The dianions were unstable on the voltammetric time scale, and a mechanism for their disappearance was suggested.

We expect that the information derived from this kinetic study will be useful for the prediction of the rates and yields of synthetically useful, electrochemically initiated homogeneous reactions. For electrosyntheses in water, or mixed aqueous solvents, experimental control of the product is usually through adjustment of pH. The systems we have described allow flexible adjustment of temperature and pressure for the liquid solvents, as well as control over dielectric constant and density in the supercritical state.

ACKNOWLEDGEMENT

The support of the Office of Naval Research (N00014-84-K-0428) is gratefully acknowledged.

REFERENCES

- (a) R. Crooks, F.-R.F. Fan and A.J. Bard, *J. Am. Chem. Soc.*, 106 (1984) 6851; (b) R. Crooks and A.J. Bard, *J. Phys. Chem.*, 91 (1987) 1274.
- (a) A.C. McDonald, F.-R.F. Fan and A.J. Bard, *J. Phys. Chem.*, 90 (1986) 196; (b) W.M. Flarsheim, Y. Tsou, I. Trachtenberg, K.P. Johnston and A.J. Bard, *J. Phys. Chem.*, 90 (1986) 3857.
- (a) G. Brunner and S. Peter, *Ger. Chem. Eng.*, 5 (1982) 181; (b) F.R. Groves, B. Bardy and F.C. Knoft, *Crit. Rev. Environ. Control*, 15 (1985) 1985; (c) K.A. Larson and M.L. King, *Biotechnol. Progress*, 2 (1986) 73; (d) M.A. McHugh and T.L. Guckes, *Macromolecules*, (1985) 674; (e) M.A. McHugh and V.J. Krukoni, *Supercritical Fluid Extraction Principles and Practice*, Butterworths, Stoneham, MA, 1986; (f) M.E. Paulaitis, V.J. Krukoni, R.T. Kurnik and R.C. Reid, *Rev. Chem. Eng.*, 1 (1983) 179; (g) D.F. Williams, *Chem. Eng. Sci.*, 36 (1981) 1769; (h) K.P. Johnston, *Kirk–Othmer Concise Encyclopedia of Chemical Technology*, Wiley, New York, 1984, p. 1141; (i) J.M.L. Penninger, M. Radosz, M.A. McHugh and V.J. Krukoni (Eds.), *Supercritical Fluid Technology*, Elsevier, Amsterdam, 1985.

- 4 S.J. Millefiori, *J. Heterocycl. Chem.*, 7 (1970) 145.
- 5 (a) K.B. Wiberg and T.P. Lewis, *J. Am. Chem. Soc.*, 92 (1970) 7154; (b) T. Fujinaga, K. Izutsu and K.J. Takaoka, *J. Electroanal. Chem.*, 12 (1966) 203.
- 6 (a) W.H. Smith and A.J. Bard, *J. Am. Chem. Soc.*, 97 (1975) 6491; (b) O.R. Brown and R.J. Butterfield, *Electrochim. Acta*, 27 (1982) 1663; (c) J. Chaudhuri, S. Kume, J. Jagur-Grodzinski and M. Szwarc, *J. Am. Chem. Soc.*, 90 (1968) 6421.
- 7 (a) O.R. Brown and R.J. Butterfield, *Electrochim. Acta*, 27 (1982) 1655; (b) R.L. Ward, *J. Am. Chem. Soc.*, 83 (1961) 3623; (c) J.E. O'Reilly and P.J. Elving, *J. Am. Chem. Soc.*, 93 (1971) 1871.
- 8 (a) R.C. Kaye and H.I. Stonehill, *J. Chem. Soc.*, (1951) 27; (b) *ibid.*, p. 2638; (c) G. Anthione, G. Coppens, J. Nasielski and E.V. Donckt, *Bull. Soc. Chim. Belg.*, 73 (1964) 65.
- 9 (a) R.J. Tabner and J.R. Yandle, *J. Chem. Soc. A*, (1968) 381; (b) C. Amatore, D. Garreau, M. Hammi, J. Pinson and J.M. Savéant, *J. Electroanal. Chem.*, 184 (1985) 1; (c) C.Z. Smith and J.H.P. Utley, *J. Chem. Research S*, (1982) 18.
- 10 A.J. Bard and L.R. Faulkner, *Electrochemical Methods*, Wiley, New York, 1980, p. 136 ff.
- 11 J.M. Savéant and E. Vianello, *C.R. Acad. Sci.*, 256 (1963) 2597.
- 12 R.S. Nicholson and I. Shain, *Anal. Chem.*, 36 (1964) 706.
- 13 J.M. Savéant and E. Vianello, *Electrochim. Acta*, 12 (1967) 629.
- 14 (a) W.V. Childs, J.T. Maloy, C.P. Keszthelyi and A.J. Bard, *J. Electrochem. Soc.*, 118 (1971) 874; (b) V.J. Puglisi and A.J. Bard, *J. Electrochem. Soc.*, 119 (1972) 829; (c) V.J. Puglisi and A.J. Bard, *J. Electrochem. Soc.*, 120 (1973) 748; (d) M.J. Hazelrigg and A.J. Bard, *J. Electrochem. Soc.*, 122 (1975) 211; (e) I. Vartires, W.H. Smith and A.J. Bard, *J. Electrochem. Soc.*, 122 (1975) 894; (f) J.M. Savéant and E. Vianello, *Electrochim. Acta*, 12 (1967) 1545; (g) C.P. Andrieux, L. Nadjo and J.M. Savéant, *J. Electroanal. Chem.*, 42 (1973) 223; (h) J.M. Savéant, C.P. Andrieux and L. Nadjo, *J. Electroanal. Chem.*, 41 (1973) 137; (i) C.P. Andrieux and J.M. Savéant, *J. Electroanal. Chem.*, 26 (1970) 223; (j) L. Nadjo and J.M. Savéant, *J. Electroanal. Chem.*, 44 (1973) 327; (k) M. Mastragostino, L. Nadjo and J.M. Savéant, *Electrochim. Acta*, 13 (1968) 721; (l) C.P. Andrieux and J.M. Savéant, *J. Electroanal. Chem.*, 33 (1971) 453; (m) V.J. Puglisi, Dissertation, University of Texas, 1972; (n) C.P. Keszthelyi, Dissertation, University of Texas, 1973; (o) M.J. Hazelrigg, Dissertation, University of Texas, 1973.
- 15 C.P. Andrieux and J.M. Savéant in C.F. Bernasconi (Ed.), *Investigations of Rates and Mechanisms of Reactions*, Vol. 6, 4/E, Part 2, Wiley, New York, 1986, p. 352.
- 16 (a) M.L. Olmstead, R.G. Hamilton and R.S. Nicholson, *Anal. Chem.*, 41 (1969) 260; (b) C.P. Andrieux, L. Nadjo and J.M. Savéant, *J. Electroanal. Chem.*, 26 (1970) 147.
- 17 C. Amatore, J. Pinson and J.M. Savéant, *J. Electroanal. Chem.*, 139 (1982) 193.
- 18 (a) V.D. Parker, *Acta Chem. Scand.*, B35 (1981) 279; (b) *ibid.*, p. 147; (c) *ibid.*, p. 149; (d) C.P. Andrieux, D.J. Brown and J.M. Savéant, *Nouv. J. Chim.*, 1 (1977) 157.
- 19 C. Amatore, J. Pinson and J.M. Savéant, *J. Electroanal. Chem.*, 137 (1982) 143.
- 20 C. Amatore, D. Garreau, M. Hammi, J. Pinson and J.M. Savéant, *J. Electroanal. Chem.*, 184 (1985) 1.
- 21 See ref. 10, (a) pp. 215–221; (b) pp. 227–229.
- 22 R.S. Nicholson, *Anal. Chem.*, 38 (1966) 1406.
- 23 K.U. Ingold in J.K. Kochi (Ed.), *Free Radicals*, Vol. 1, Wiley, New York, 1973, pp. 37–112.
- 24 M.L. Morrell and G. Vincow, *J. Am. Chem. Soc.*, 91 (1969) 6389.